Synsint Research Group

Available online at www.synsint.com

Synthesis and Sintering

**ISSN** 2564-0186 (Print), **ISSN** 2564-0194 (Online)

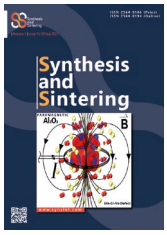

*Research article*

# Ab-initio study of paramagnetic defects in Mn and Cr doped transparent polycrystalline $Al_2O_3$ ceramics

**Mubashir Mansoor** [a,b,*], **Mehya Mansoor** [a,c], **Maryam Mansoor** [a,d], **Zuhal Er** [b,e], **Filiz Çinar Şahin** [a]

[a] *Department of Metallurgical and Materials Engineering, Istanbul Technical University, Maslak 34467, Istanbul, Turkey*
[b] *Department of Applied Physics, Istanbul Technical University, Maslak 34467, Istanbul, Turkey*
[c] *Department of Geological Engineering, Istanbul Technical University, Maslak 34467, Istanbul, Turkey*
[d] *Department of Mining Engineering, Istanbul Technical University, Maslak 34467, Istanbul, Turkey*
[e] *Faculty of Maritime, Istanbul Technical University, Tuzla 34940, Istanbul, Turkey*

A B S T R A C T

Birefringence is a major source of difficulty in sintering of transparent polycrystalline alumina ceramics, especially as the grain size exceeds a few hundred nanometers, which ultimately leads to complete opacity, mainly due to scattering of light. Recent studies have made it clear that by application of a strong magnetic field, alumina grains can be aligned along a particular crystallographic orientation, which minimizes scattering due to birefringence, and enhances transparency. Defects that cause spin delocalization are known to induce a paramagnetic behavior in alumina ceramics. Therefore, such defects have become a focal point of research for magnetic field assisted sintering of transparent polycrystalline alumina, in order to reduce the necessary magnetic field strength during production process. In light of recent studies on paramagnetic potentials of transition metal doped alumina, we have applied Spin Polarized Density Functional Theory (SP-DFT) calculations on manganese and chromium doped and co-doped alumina to calculate the magnetic moments, density of states and defect formation energies, which should be expected from this system of dopants, along with their interactions with oxygen vacancies. The results clearly indicate that formation of a point defect comprised of chromium and manganese positioned substitutionally at adjacent aluminum sites, in vicinity of an oxygen vacancy can induce a magnetic moment equivalent to 5 Bohr magnetons ($\mu_B$), outperforming previously reported defects. Based on this study we find it likely that chromium and manganese co-doping in alumina can further reduce the required magnetic field strength for production of transparent polycrystalline alumina.



KEYWORDS

DFT
Transparent ceramics
Sintering
Alumina
Paramagnetic ceramics

OPEN ACCESS

## 1. Introduction

Polycrystalline alumina and single crystal sapphire are extensively used in the power electronic devices [1], information and communication technologies [2], aerospace and defense industries [3], mobile phone devices [4], fingerprint sensors and cameras [5], and metal-oxide-semiconductor (MOS) integrated circuit (IC) as in silicon on sapphire (SOS) [6, 7]. Not to mention the centuries old use of sapphire as a precious gemstone. Recent advances on nanofluids containing alumina are also reported to be effective for heat sink applications with considerable increase in thermal conductivity when compared with

* Corresponding author. *E-mail address:* mansoor17@itu.edu.tr (M. Mansoor)
Received 26 July 2021; Received in revised form 13 September 2021; Accepted 13 September 2021.
Peer review under responsibility of Synsint Research Group. 
https://doi.org/10.53063/synsint.2021.1340

plain water [8], making alumina a highly versatile material for a wide range of applications. The transparency of alumina ranges from approximately 200 nm to 4000 nm due to its wide band gap of approximately 9 eV [9, 10], making this material exceptional for many optical applications, such as lasers (with appropriate dopants), lenses, screens, and windows [5]. Alumina is also an excellent electrical insulator, preventing leakage currents in electric and electronic devices [11]. It exhibits outstanding performance under demanding conditions, as in corrosive media & high temperatures [12, 13]. The tribological properties and a hardness next to diamond has made alumina, in either polycrystalline or single crystal form, the ceramic of choice for applications requiring exceptional optical behavior, even as a transparent abrasion resistant material [5]. It is therefore, of great importance to easily produce novel alumina components economically, in order to maximize its use for demanding applications.

Producing transparent alumina is not simple, mainly due to this material's anisotropic optical behavior [14]. Considering a polycrystalline solid with random grain orientations, the incoming light must pass through crystallites of slightly different refractive index, which would result in absorption of light, eventually making the material opaque despite the absence of porosities or any other scattering centers [15]. An age-old solution to this problem has been growing single crystal alumina (sapphire), in spite of the difficulties and expenses associated with the process [16]. Given that the main culprit, in case of optical applications of polycrystalline alumina, is the crystal's anisotropic optical behavior or birefringence [14], sintering of transparent polycrystalline alumina has become a serious challenge for the advanced ceramics industry. Recent advances in the production of transparent polycrystalline alumina are opening up a new era of affordable solutions, which were traditionally not possible [17–19]. A development in this regard was brought forward through controlling the alumina microstructure by rapid sintering techniques such as Spark Plasma Sintering (SPS), which can avoid excessive grain growth during sintering, due to short dwell times of only a few minutes. The main benefit of SPS is its ability to achieve densification without allowing excessive grain growth [20]. Although SPS is generally regarded as an efficient technique for sintering of electrically conductive material, a wide range of research work has shown its capabilities for producing monolithic electrically insulating ceramics as well [14, 20–22]. The application of SPS for sintering of monolithic alumina with a grain size of less than the visible wavelength of light had made it possible to minimize scattering substantially, and thus enhance transparency [18, 20]. Although, SPS is a revolutionary technique, the combination of requirements for an extremely rapid sintering process, which can also facilitate sufficient densification, and flexibility in achievable ceramic shapes, has been a serious enough challenge to avoid industrial-scale use of transparent nano-grained alumina ceramics for electronic and optical applications. It is therefore necessary to develop alternative techniques based on more conventional sintering processes for mass production of such ceramics.

An ingenious method has been proposed over the past few years by several research groups [19, 23, 24] for preparing the green body of alumina ceramics by slip casting, under a strong enough magnetic field to facilitate a directional orientation of the grains prior to sintering. They have proposed texturing the ceramic such that the grains are aligned in the same crystallographic orientation, thereby solving the absorption issue due to birefringence, which is mainly caused by random distribution of grains. A strong magnetic field can potentially re-orient the grains along the same optical axis [19]. The technique has proved to be extremely successful, making it possible to sinter transparent alumina ceramics which are comparable with single crystal sapphire in terms of their optical quality, while having a polycrystalline structure with large grain sizes of approximately 30 to 50 microns [24]. A feat of remarkable importance, which should not be taken lightly. The problem with this technique is the necessity for extremely strong magnetic fields; generally in excess of 10 Tesla. Moreover, slip casting is not capable of producing intricate shapes, which further hinders widespread use of this technique. In other words, the main problem is the diamagnetic nature of alumina. As a solution to this problem, Nykwest and Alpay [25, 26] have proposed doping alumina such that the net magnetic moment of the grains increases significantly and thus reducing the requirements for a strong magnetic field. They have shown that doping alumina with transition metals, especially chromium and manganese is capable of inducing 3 $\mu_\beta$ of magnetic moment in alumina by creating delocalized orbitals with a net difference in the spin-up and spin-down electron density of states. Doping alumina for inducing paramagnetism, makes magnetic field assisted sintering of the material easier, and increases the optical qualities while potentially reducing process cost. It also opens up the conversation for possibilities of such alumina ceramics, as paramagnetic sensors and electronic device components. It is customary to think of alumina or sapphire as an electrically insulator diamagnetic material, however, recent advances in this regard are showing potentials in producing alumina ceramics which can be highly tailored for electronic and optical requirements of the industry, especially through atomic scale materials design by application of powerful ab-initio approaches including DFT [26].

An additional challenge in the production of transparent polycrystalline alumina is a gray coloration, which emerges upon sintering in SPS or hot isostatic press (HIP) equipment, which can be decolorized only through subsequent heat treatments [27]. The exact cause of this phenomena is not very well understood, however there are several hypotheses in this regard. It has been reported that the gray coloration is a result of carbon diffusion or precipitation in the ceramic, at ppm level, which causes this nefarious optical behavior. Conversely recent reports by Morita et al. [28] have made it clear that the coloration cannot be diffusion related. Other possibilities for the cause of gray coloration include oxygen vacancy point defects [27], and nano-sized precipitation of impurities. The latter is readily seen in natural sapphires that are heated under extremely low oxygen partial pressures, where precipitation of iron nanocrystals becomes inevitable [29, 30]. However further research is necessary as the present literature does not present a conclusive mechanism in this regard.

The aim of this study is to explore the magnetic moments induced by defects in manganese and chromium doped and co-doped alumina powder, in order to search for defects that can increase the magnetic moments even further, as well as providing a qualitative investigation on the likelihood of calculated defects under oxygen rich or poor conditions. Moreover, it is known that the application of high-energy irradiation or heat treatments under low oxygen partial pressure can induce vacancies in the precursor alumina powder [31]. Therefore, we have investigated the impacts of vacancy-bearing defect complexes on the magnetic moment of Cr and Mn doped, and co-doped alumina ceramics, by using first principles approach of DFT.

## 2. Computational method

Spin polarized density functional theory has been applied using the Generalized Gradient Approximation, as parametrized by Perdew, Burke and Ernzerhof (GGA-PBE) [32]. A supercell size of 2×2×1 (120 atoms in case of pristine crystal) has been used under periodic boundary conditions, which is known to be large enough to almost eliminate the spurious defect-defect interactions [10]. Geometry optimizations have been carried out under a constant cell volume with a plane wave cut-off energy of 500 eV, k-point spacing of 0.5 per angstrom (k-mesh grid of 3×3×1) and Gaussian smearing of 0.05 eV with SCF convergence threshold of $10^{-5}$ eV. The atoms have been relaxed until forces are less than 0.02 eV/Å. Density of state and charge densities are calculated with a higher k-mesh grid of 5×5×3 and origin shifted to gamma. Calculations have been carried out using Projector Augmented Wave pseudopotentials (PAW) [33] as implemented in Vienna ab-initio software package (VASP 6.1) under the framework of MedeA [34–36]. Magnetization densities have been calculated for the pristine supercell, and cells containing neutral Mn, Cr, Mn-Cr, Mn-Vo, Cr-Vo and Mn-Cr-Vo defects, where Vo represents an oxygen vacancy, with the transition metals positioned in substitutional aluminum sites. Defect formation energy (E) has been calculated using Eq. 1, as proposed by Zhang and Northrup [37], and Van de Walle [38].

$$E = E_{def} - E_{pure} - \sum N\mu_i \quad (1)$$

$E_{def}$ and $E_{pure}$ represent the formation energy of the defective and pristine supercells respectively. Contribution of the Fermi energy is not included given that the defects studied are charge neutral. N is the number of atom(s) i removed from or added to the supercell, with μ representing the chemical potential of the added or removed atom. The chemical potentials depend on the partial pressure of oxygen, absolute pressure and temperature [38]. However, the lower and upper bounds of the $\mu_{Al}$ and $\mu_O$ are defined by Eq. 2, which satisfies the thermodynamic boundaries for stability of the alumina phase at P = 0 atm. Given that sintering of transparent alumina ceramics are generally carried out using HIP or SPS equipment, which are operating under relatively low partial pressures of oxygen (Al-rich conditions), $\mu_{Al}$ is taken as the DFT calculated formation energy of bulk aluminum metal. The oxygen chemical potential is found accordingly based on Eq. 2, where $\mu_{Al2O3}$ is the formation energy of a stoichiometric pristine alumina as calculated by DFT. Under such oxygen deprived conditions, the chemical potentials of chromium and manganese are also based on the DFT calculated formation energies of their respective metallic structures.

$$\mu_{Al_2O_3} = 2\mu_{Al} + 3\mu_O \quad (2)$$

In the case of high oxygen partial pressure limit (O-rich), the chemical potential of aluminum is deduced based on Eq. 2, using half the DFT calculated energy of oxygen molecule, as the oxygen chemical potential. The values for $\mu_{Cr}$ and $\mu_{Mn}$ have been estimated from the formation energies of $Cr_2O_3$ and $MnAl_2O_4$ respectively, which are the compatible phases with alumina, based on their respective phase equilibria [39, 40]. Calculated formation energies are valid for zero kelvin temperature, and should serve the purpose of a qualitative comparison only. It is possible to evaluate the impact of higher temperatures and intermediate partial pressures of gases on the formation energies, using statistical mechanics as shown in the literature [38, 41]. However, for the purpose of this study, the defect formation energies are only used as estimates for a comparison between the defects at low temperatures, prior to sintering. Therefore, the impact of temperature has not been included. Nevertheless, it should be noted that based on Eq. 1 and Eq. 2, the defect formation energies are highly dependent on furnace atmosphere, temperature, pressure and presence of other complex or charged defects in the crystal, which can change the equilibrium Fermi level and thus significantly impact the defect equilibria [41–43]. Given that calculation of complex and charged defects are essential for; plotting Kroger-Vink diagrams, estimating defect concentrations and finding solubility limits of dopants, it is not possible to accurately deduce such information based on calculations done in this study, and as the main purpose of this paper is to find the induced magnetic moments by the defects mentioned above, we have refrained from doing a detailed analysis of defect equilibria. However, given the results mentioned in the following section, such analysis is highly recommended.

## 3. Results and discussion

The total and partial density of states are shown in Fig. 1. The Fermi energy is set to 0 eV, representing the highest occupied level, and the calculated band gap of the pure crystal is found to be 6.17 eV, with the enthalpy of formation (T = 0 K) being -14.97 eV, which are in agreement with prior theoretical studies using GGA-PBE functional [41, 44]. The discrepancy between the calculated and experimental band gap is due to the used functional, which is a well-established shortcoming of DFT [45], however, given that the levels have a systematic error, makes it possible to interpret the data efficiently, by considering appropriate band edges and referencing Fermi level to a common potential rather than valence band maximum [46]. Each of the proposed defects cause deep levels in the band gap, with significant contributions from d-orbitals, except in $V_O$. The total density of states for spin up and spin down electrons shows significant difference in all of the transition metal containing defects, thus causing a net magnetic moment. Although it is possible to correct for this systematic error in DOS through higher levels of theory [45], the energy levels reported using DFT are not considerably erroneous for the purpose of this study, as shown by Somjit and Yildiz [41]. Nevertheless, the optical transitions cannot be deduced using reported DOS, given that a more accurate evaluation of the energy levels becomes necessary for describing absorption and emission wavelengths. Moreover, the phononic contribution is not negligible in alumina, as calculated by Na-Phattalung [10] in the case of Cr-doped alumina, and since there is no reason to believe other defects will be any different, calculation of configuration coordinate diagrams becomes essential in this regard. Although single substitutional chromium is a well-known chromophore, considering the energy levels shown by DOS plots, it is possible to say that the other defects reported here are potential chromophores as well and further hybrid functional calculations are necessary to shed light on absorption or emission wavelengths, which may arise due to these defects. It is noteworthy that all of the calculated defects exhibited a red shift in the onset of absorption spectrum, with significant contributions from the d-orbitals in the case of single substitutional Mn defect, as shown in Fig. 1d.

An additional finding worth noting is that the number of levels induced by Cr-Mn defect is rather high, with possible transitions in the infrared region, thus making chromium and manganese co-doped alumina, a potential material for absorption in the IR region.

Considering the calculated DOS for $V_O$ defect, it is also possible to rule out the hypothesis put forth by Wei [27], regarding gray coloration of transparent alumina ceramics during sintering being a consequence of oxygen vacancies. The distinct energy levels produced by this defect are not capable of causing an absorption continuum, which is necessary for formation of a gray shade, and one should only expect distinct wavelengths of the absorption and emission from this defect. Our finding in this regard is in qualitative agreement with prior work by Pustovarov et al. [47], therefore, leaving the question for the cause of gray as-sintered polycrystalline alumina open for debate and further research.

The magnetic moments and formation energies of defects under lowest $pO_2$ limit (Al-Rich) and highest $pO_2$ limit (O-Rich) are given in Table 1. The results for the formation energies are in reasonable agreement with the HSE functional calculations of Na-Phattalung et al. [10], which further signifies the conclusions of Somjit and Yildiz [41] regarding applicability of GGA-PBE functional for the purpose of defect thermodynamics in alumina. Not surprisingly, under Al-rich conditions, the formation energy of oxygen vacancy is lowest amongst these defects; therefore, $V_O$ is expected to form in considerable concentrations upon sintering at the lowest limits of oxygen partial pressure. However, this defect does not induce any measurable paramagnetism and is therefore not particularly useful in aiding the orientation of grains in green body, or during sintering, upon application of a magnetic field. On the other hand, as reported by Nykwest and Alpay [25], chromium is indeed an excellent choice as it has a complete solubility in alumina at higher oxygen partial pressures, and significant solubility even at reduced $pO_2$, apparent from the Al-rich defect formation energy, as well as a fair magnetic moment of $3\mu_\beta$. Manganese has also been reported to be an ideal dopant [26]. We have found a defect formation energy of 4.36 eV at low $pO_2$, unlike the formation energies reported in oxygen rich conditions, which means, the solubility of manganese in alumina is very much dependent on the partial pressure of oxygen, as is in the case with iron [48]. Therefore, precipitation of manganese is likely at low $pO_2$ during sintering, if the Mn concentration is close to solubility limit of high $pO_2$. Co-doping chromium and manganese can lead to a plethora of defects, and every possible defect has not been considered in this study, however, it is possible to note that despite this concern over solubility limits of Mn, the Cr-Mn-Vo defect, which is comprised of chromium and manganese atoms positioned at adjacent aluminum sites, next to an oxygen vacancy, shows a magnetic moment of 5 $\mu_\beta$, better by approximately 67% when comparing with a single substitutional chromium defect in alumina and outperforming the previously reported defects by Nykwest and Alpay [25, 26]. Although the magnetic properties induced by the Cr-Mn-$V_O$ defect is rather attractive, the formation energy of this defect is not low enough, to form at significant concentrations during sintering at low $pO_2$, by virtue of thermodynamic equilibrium. As a solution to this problem, one might consider non-equilibrium processes, which induce vacancies, so that a high enough concentration of this defect may form at room temperature, making it easier for the grains in the green body to be aligned along a single crystallographic orientation under a weaker magnetic field. As an example of such processes, high-energy neutron bombardment may be considered, which is known to result in formation of vacancies in alumina [31]. Therefore, based on this theoretical study, it is anticipated that high energy irradiation of chromium and manganese co-doped alumina powder should cause significant paramagnetic behavior at room temperature, making it possible to reduce the required magnetic field strength for crystallographic alignment of the grains in green body. It is also noteworthy that considering the energies reported in Table 1, inducing vacancy is not always a good strategy for increasing the magnetic moment of alumina, but through proper dopants, vacancies can have important contributions in this regard.

An additional factor, which can determine the potential efficiency of the induced magnetic moment, is the spatial distribution of the magnetization density, which is considered to be an important factor in texturing of the ceramics. Our results in this regard are shown in Fig. 2. The results for Cr and Mn defects are consistent with earlier reports by Nykwest and Alpay [25], however, the Cr-Mn-Vo and Vo defects create a relatively more de-localized magnetization density, in comparison to other defects reported in this study, which is an additional factor aiding in the directional orientation of grains. Based on the results, one wonders the impact of using magnetic field during sintering, especially upon incorporation of a transient liquid phase, which could further facilitate alignment of the grains along the same crystallographic axis. At room temperature, one can create the Cr-Mn-Vo defect through neutron bombardment of Cr-Mn doped precursor alumina powder, followed by sintering under a weaker magnetic field where Cr defects will be highly stable and sufficiently capable in

**Table 1**. Magnetic moments are given in the unit of Bohr Magnetons, and defect formation energies are mentioned in eV, for the zero Kelvin temperature under an aluminum rich (lowest $pO_2$) and oxygen rich (highest $pO_2$) conditions. The third column refers to first two terms of Eq. 1, as calculated by DFT.

| Defect type | Magnetic moment ($\mu_\beta$) | $E_{def}$–$E_{pure}$ (eV) | Formation energy Al-rich (eV) | Formation energy O-rich (eV) |
|---|---|---|---|---|
| **Pure crystal** | 0.0008 | N/A | N/A | N/A |
| **Vo** | 0.0016 | 11.67 | 1.75 | 6.74 |
| **Cr** | 3.0000 | -2.69 | 2.99 | -0.08 |
| **Cr-Vo** | 3.0000 | 8.31 | 4.07 | 5.99 |
| **Mn** | 2.0000 | -0.78 | 4.36 | -3.06 |
| **Mn-Vo** | 2.0000 | 9.66 | 4.88 | 2.45 |
| **Cr-Mn** | 1.0000 | -3.50 | 7.32 | -3.17 |
| **Cr-Mn-Vo** | 5.0000 | 6.97 | 7.87 | 2.37 |

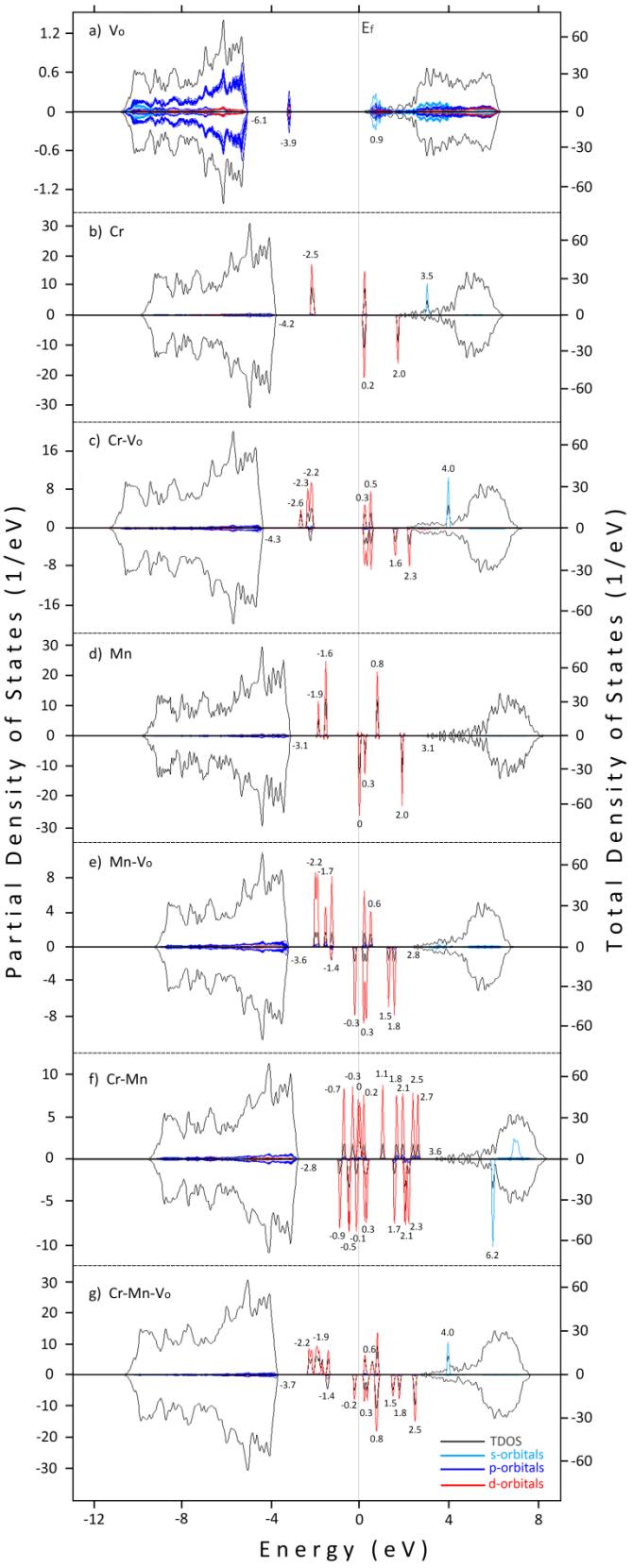


**Fig. 1.** Total and partial density of states for a) Vo, b) Cr, c) Cr-Vo, d) Mn, e) Mn-Vo, f) Cr-Mn, and g) Cr-Mn-Vo defects. The Fermi level is set to 0 eV and alignment is done accordingly. Black line represents the DOS (right axis) and colored lines represent partial DOS (left axis). The inscribed numbers are energies associated with each state, correct to one decimal place.

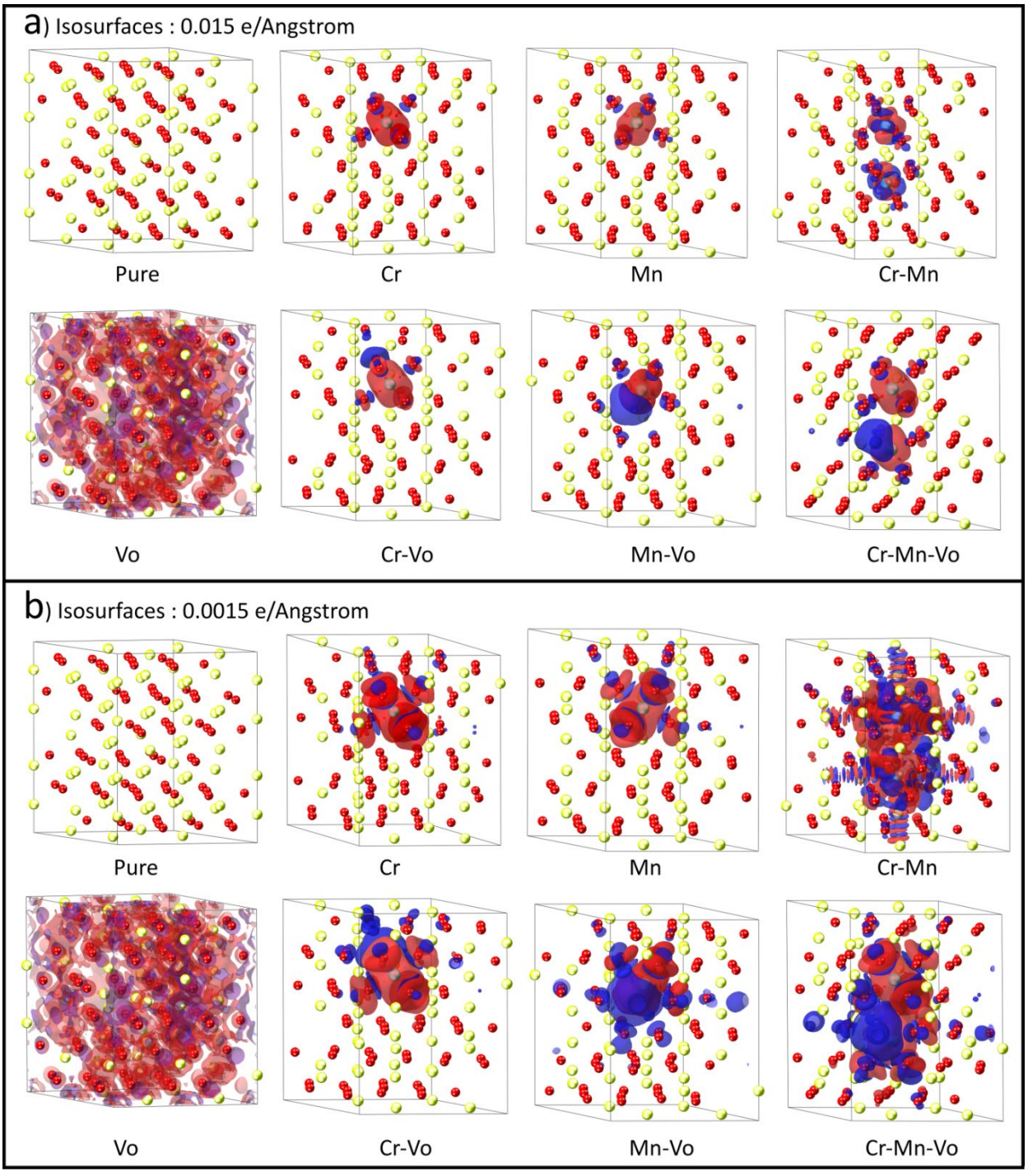


**Fig. 2.** Magnetization density are shown with isosurfaces of a) 0.015 e/A, and b) 0.0015 e/A. Spin up and down electrons are shown by red and blue surfaces respectively. Yellowish green and red color solid spheres represent aluminum and oxygen atoms respectively. Oxygen vacancy and Cr-Mn-Vo defects have the highest magnetization density.

inducing paramagnetism, making it possible to get one step closer to economical industrial scale production of transparent polycrystalline alumina.

## 4. Conclusions

Our DFT calculations on manganese and chromium doped and co-doped alumina have made the following points clear:

- Oxygen vacancy cannot be the cause of gray coloration in as-sintered transparent alumina.
- Inducing oxygen vacancy is not always an effective strategy for increasing magnetic moment in alumina.
- Solubility of manganese in alumina is dependent on oxygen partial pressure, and decreases with lowering $pO_2$.
- Co-doping manganese and chromium in alumina powder followed by neutron irradiation makes formation of Mn-Cr-Vo defect likely, substantially increasing the magnetic moment (5 $\mu_\beta$), thereby requiring a lower magnetic field strength during alignment of crystallographic orientations of grains in green body, resulting in increased optical quality of sintered transparent alumina.
- Based on the calculated DOS, Mn-Cr co-doped alumina is expected to show absorption of light in infrared and visible wavelengths, causing coloration. Further calculations by hybrid functionals are necessary in this regard.

## CRediT authorship contribution statement

**Mubashir Mansoor:** Conceptualization, Methodology, Writing – original draft.
**Mehya Mansoor:** Investigation, Writing – original draft.
**Maryam Mansoor:** Investigation, Writing – original draft.
**Zuhal Er:** Funding acquisition, Writing – review & editing.
**Filiz Çinar Şahin:** Supervision, Writing – review & editing.

## Data availability

The data underlying this article will be shared on reasonable request to the corresponding author.

## Declaration of competing interest

The authors declare no competing interests.

## Funding and acknowledgment

The fruitful discussions with Professor Kamil Czelej, Professor Mustafa Ürgen, Professor Servet Timur, and Dr. Réné Windiks have been an integral part of this study, for which we are very thankful. We would also like to acknowledge the supercomputer support of the National Center for High Performance Computing of Turkey (UHeM), for facilitating the calculations in this study, under grant number 1008852020.

## References

[1] W. Saito, T. Nitta, Y. Kakiuchi, Y. Saito, K. Tsuda, et al., On-resistance modulation of high voltage gan hemt on sapphire substrate under high applied voltage, IEEE Electron Device Lett. 28 (2007) 676–678. https://doi.org.10.1109/led.2007.901665.
[2] G. Bakshi, A. Vaish, R.S. Yaduvanshi, Two-Layer sapphire Rectangular dielectric Resonator antenna for Rugged Comunications, Prog. Electromagn. Res. Lett. 85 (2019) 73–80. https://doi.org/10.2528/pierl19030602.
[3] C.P. Khattak, R. Shetty, C.R. Schwerdtfeger, S. Ullal, World′s largest sapphire for many applications, J. Cryst. Growth. 452 (2016) 44–48. https://doi.org/10.1016/j.jcrysgro.2015.11.026.
[4] G. Lin, Y. Huang, High mechanical strength sapphire cover lens for smartphone screen, Cryst. Res. Technol. 53 (2018) 1800049. https://doi.org/10.1002/crat.201800049.
[5] V. Pishchik, L.A. Lytvynov, E.R. Dobrovinskaya, Sapphire: Material, Manufacturing, Applications (Micro- and Opto-Electronic Materials, Structures, and Systems, Springer, New York, NY. (2009). https://doi.org/10.1007/978-0-387-85695-7.
[6] S. Cristoloveanu, Silicon Films on Sapphire, Rep. Prog. Phys. 50 (1987) 327–371. https://doi.org/10.1088/0034-4885/50/3/002.
[7] W.M. Yim, R.J. Paff, Thermal expansion of ALN, Sapphire, and Silicon, J. Appl Phys. 45 (1974) 1456–1457. https://doi.org/10.1063/1.1663432.
[8] M. Ataei, F. Sadegh Moghanlou, S. Noorzadeh, M. Vajdi, M. Shahedi Asl, Heat transfer and flow characteristics of hybrid Al2O3/TiO2–water nanofluid in a minichannel heat sink, Heat Mass Transf. 56 (2020) 2757–2767. https://doi.org/10.1007/s00231-020-02896-9.
[9] R.H. French, D.J. Jones, S. Loughin, Interband electronic structure Of alpha-Alumina up to 2167 K, J. Am. Ceram. Soc. 77 (1994) 412–422. https://doi.org/10.1111/j.1151-2916.1994.tb07009.x.
[10] S. Na-Phattalung, S. Limpijumnong, J. T-Thienprasert, First-principles study of chromium defects in α-Al2O3: The Origin of Red Color in ruby, Phys. Status Solidi B. 257 (2020) 2000159. https://doi.org/10.1002/pssb.202000159.
[11] G.P. Imthurn, G.A. Garcia, H.W. Walker, L. Forbes, Bonded silicon-on-sapphire wafers and devices, J. Appl. Phys. 72 (1992) 2526–2527. https://doi.org/10.1063/1.352345.
[12] M. Soeda, T. Kataoka, Y. Ishikura, S. Kimura, T. Masuda, et al., Sapphire-based capacitive pressure sensor for high temperature and harsh environment application, Proc. IEEE Sens. (2002). https://doi.org/10.1109/icsens.2002.1037237.
[13] Y. Zhang, G. Pickrell, B. Qi, A. Safaai-Jazi, A. Wang, Single-crystal sapphire based optical polarimetric sensor for high temperature measurement, Sensors. 6 (2006) 823–834. https://doi.org/10.3390/s6080823.
[14] L.B. Kong, Y.Z. Huang, W.X. Que, T.S. Zhang, S. Li, et al., Transparent ceramics, Topics in Mining, Metallurgy and Materials Engineering, Springer Cham. (2015). https://doi.org/10.1007/978-3-319-18956-7.
[15] R. Apetz, M.P. Bruggen, Transparent alumina: A light-scattering model, Journal of the American Ceramic Society. 86 (2003) 480–486. https://doi.org/10.1111/j.1151-2916.2003.tb03325.x.
[16] B. Cockayne, M. Chesswas, D.B. Gasson, Single-crystal growth of sapphire, J. Mater. Sci. 2 (1967) 7–11. https://doi.org/10.1111/j.1151-2916.2003.tb03325.x.
[17] M. Trunec, K. Maca, R. Chmelik, Polycrystalline alumina ceramics doped with nanoparticles for increased transparency, J. Eur. Ceram. Soc. 35 (2015) 1001–1009. https://doi.org/10.1016/j.jeurceramsoc.2014.09.041.
[18] A. Belenky, I. Bar-On, D. Rittel, Static and dynamic fracture of transparent nanograined alumina, J. Mech. Phys. Solids. 58 (2010) 484–501. https://doi.org/10.1016/j.jmps.2010.02.002.
[19] T. Ashikaga, B.-N. Kim, H. Kiyono, T.S. Suzuki, Effect of crystallographic orientation on transparency of alumina prepared using magnetic alignment and SPS, J. Eur. Ceram. Soc. 38 (2018) 2735–2741. https://doi.org/10.1016/j.jeurceramsoc.2018.02.006.
[20] B. Apak, G. Göller, Y. Onüralp, F.Ç. Şahin, The effects of codoping Y2O3 on MgO doped spark plasma sintered Al2O3, Adv. Sci. Technol. 63 (2010) 74–78. https://doi.org/10.4028/www.scientific.net/AST.63.74.
[21] L. Liu, K. Morita, T.S. Suzuki, B.-N. Kim, Effect of the heating rate on the Spark-Plasma-Sintering (SPS) of Transparent Y2O3 Ceramics: Microstructural Evolution, mechanical and optical properties, Ceramics. 4 (2021) 56–69. https://doi.org/10.3390/ceramics4010006.
[22] F.C. Sahin, H.E. Kanbur, B. Apak, Preparation of AlON Ceramics via reactive Spark Plasma Sintering, J. Eur. Ceram. Soc. 32 (2012) 925–929. https://doi.org/10.1016/j.jeurceramsoc.2011.10.043.
[23] X. Mao, S. Wang, S. Shimai, J. Guo, Transparent polycrystalline alumina ceramics with orientated optical axes, J. Am. Ceram. Soc.

91 (2008) 3431–3433. https://doi.org/10.1111/j.1551-2916.2008.02611.x.
[24] H. Yi, X. Mao, G. Zhou, S. Chen, X. Zou, et al., Crystal plane evolution of grain oriented alumina ceramics with high transparency, Ceram. Int. 38 (2012) 5557–5561. https://doi.org/10.1016/j.ceramint.2012.03.074.
[25] E.C. Nykwest, S.P. Alpay, Towards magnetic alumina: Uncovering the roles of transition metal doping and electron hybridization in spin delocalization, J. Phys.: Condens. Matter. 31 (2019) 245801. https://doi.org/10.1088/1361-648x/ab0fe4.
[26] E.C. Nykwest, B. Christopher Rinderspacher, J.M. Elward, R.E. Brennan, K.R. Limmer, Magnetic and energetic properties of transition metal doped alumina, J. Phys.: Condens. Matter. 30 (2018) 395801. https://doi.org/10.1088/1361-648x/aada2a.
[27] G.C. Wei, Transparent ceramics for lighting, J. Eur. Ceram. Soc. 29 (2009) 237–244. https://doi.org/10.1016/j.jeurceramsoc.2008.03.018.
[28] K. Morita, B.-N. Kim, H. Yoshida, K. Hiraga, Y. Sakka, Distribution of carbon contamination in oxide ceramics occurring during spark-plasma-sintering (SPS) processing: II - effect of SPS and loading temperatures, J. Eur. Ceram. Soc. 38 (2018) 2596–2604. https://doi.org/10.1016/j.jeurceramsoc.2017.12.004.
[29] A.R. Moon, M.R. Phillips, Iron and Spinel precipitation IN Iron-Doped Sapphire, J. Am. Ceram. Soc. 74 (1991) 865–868. https://doi.org/10.1111/j.1151-2916.1991.tb06943.x.
[30] J.L. Emmett, T.R. Douthit, Heat treating the Sapphires of Rock creek, montana, Gems Gemol. 29 (1993) 250–272. https://doi.org/10.5741/gems.29.4.250.
[31] G.P. Pells, Radiation damage effects in alumina, J. Am. Ceram. Soc. 77 (1994) 368–377. https://doi.org/10.1111/j.1151-2916.1994.tb07004.x.
[32] J.P. Perdew, M. Ernzerhof, K. Burke, Rationale for mixing exact exchange with density functional approximations, J. Chem. Phys. 105 (1996) 9982–9985. https://doi.org/10.1063/1.472933.
[33] G. Kresse, D. Joubert, From Ultrasoft pseudopotentials to the projector augmented-wave method, Phys. Rev. B. 59 (1999) 1758–1775. https://doi.org/10.1103/PhysRevB.59.1758.
[34] G. Kresse, M. Marsman, J. Furthmüller, VASP the Guide. (2018).
[35] MedeA version 3.2.2; MedeA is a registered trademark of Materials Design, Inc., San Diego, USA.
[36] G. Kresse, J. Furthmüller, Efficient Iterative Schemes Forab initiototal-energy calculations using a plane-wave basis set, Phys. Rev. B. 54 (1996) 11169–11186. https://doi.org/10.1103/PhysRevB.54.11169.
[37] S. Zhang, J. Northrup, Chemical potential dependence of defect formation energies in GaAs: Application to Ga self-diffusion, Phys. Rev. Lett. 67 (1991) 2339–2342. https://doi.org/10.1103/PhysRevLett.67.2339.
[38] C.G. Van de Walle, D.B. Laks, G.F. Neumark, S.T. Pantelides, First-principles calculations of solubilities and doping limits: Li, Na, and N in ZnSe, Phys. Rev. B. 47 (1993) 9425–9434. https://doi.org/10.1103/PhysRevB.47.9425.
[39] K.T. Jacob, Revision of thermodynamic data on MnO–Al2O3Melts, Can. Metall. Quart. 20 (1981) 89–92. https://doi.org/10.1179/cmq.1981.20.1.89.
[40] A. Muan, S. Somiya, Phase equilibrium studies in the system iron oxide-Al2O3-Cr2O3, J. Am. Ceram. Soc. 42 (1959) 603–613. https://doi.org/10.1111/j.1151-2916.1959.tb13581.x.
[41] V. Somjit, B. Yildiz, Doping α-Al2O3 to reduce its hydrogen permeability: Thermodynamic assessment of hydrogen defects and solubility from first principles, Acta Mater. 169 (2019) 172–183. https://doi.org/10.1016/j.actamat.2019.02.031.
[42] A. Zunger, O.I. Malyi, Understanding doping of quantum materials, Chem. Rev. 121 (2021) 3031–3060. https://doi.org/10.1021/acs.chemrev.0c00608.
[43] M. Youssef, B. Yildiz, Intrinsic point-defect equilibria in tetragonal ZrO2: Density functional theory analysis with finite-temperature effects, Phys. Rev. B. 86 (2012). https://doi.org/10.1103/PhysRevB.86.144109.
[44] G. Zhang, Y. Lu, X. Wang, Hydrogen interactions with intrinsic point defects in hydrogen permeation barrier of α-Al2O3: A first-principles study, Phys. Chem. Chem. Phys. 16 (2014) 17523. https://doi.org/10.1039/C4CP01382D.
[45] C. Freysoldt, B. Grabowski, T. Hickel, J. Neugebauer, G. Kresse, et al., First-principles calculations for point defects in solids, Rev. Mod. Phys. 86 (2014) 253–305. https://doi.org/10.1103/RevModPhys.86.253.
[46] A. Alkauskas, P. Broqvist, A. Pasquarello, Defect levels through hybrid density functionals: Insights and applications, Phys. Status Solidi B. 248 (2011) 775–789. https://doi.org/10.1002/pssb.201046195.
[47] V.A. Pustovarov, T.V. Perevalov, V.A. Gritsenko, T.P. Smirnova, A.P. Yelisseyev, Oxygen vacancy in Al2O3: Photoluminescence Study and first-principle simulation, Thin Solid Films. 519 (2011) 6319–6322. https://doi.org/10.1016/j.tsf.2011.04.014.
[48] H.-Y. Lee, Y.-W. Rhee, S.-J.L. Kang, Discontinuous dissolution and grain-boundary migration in Al2O3-Fe2O3 by oxygen partial pressure change, J. Am. Ceram. Soc. 79 (1996) 1659–1663. https://doi.org/10.1111/j.1151-2916.1996.tb08778.x.